



Research Paper

Overexpression of ULK1 Represents a Potential Diagnostic Marker for Clear Cell Renal Carcinoma and the Antitumor Effects of SBI-0206965



Jun Lu ^{a,*}, Ling Zhu ^{a,1}, Luo-ping Zheng ^{b,1}, Qiang Cui ^{c,1}, He-huan Zhu ^a, Hu Zhao ^a, Zhou-ji Shen ^d, Hui-yue Dong ^a, Shu-shang Chen ^a, Wei-zhen Wu ^{a,*}, Jian-ming Tan ^{a,*}

^a Fujian Provincial Key Laboratory of Transplant Biology, Fuzhou General Hospital or Dongfang Hospital, Xiamen University, Fuzhou, China

^b Department of Urology, The Affiliated Sanming First Hospital of Fujian Medical University, Sanming, China

^c Nephrology and Urology Department, The Second Affiliated Hospital of Wannan Medical College, Wuhu, China

^d Nephrology Department, Ningbo Medical Centre Lihuilili Eastern Hospital, Ningbo, China

ARTICLE INFO

Article history:

Received 10 April 2018

Received in revised form 24 July 2018

Accepted 24 July 2018

Available online 2 August 2018

Keywords:

Clear cell renal carcinoma (ccRCC)

SBI-0206965

ULK1

ABSTRACT

Background: Uncoordinated 51-like kinase 1 (ULK1) plays a vital role in autophagy. ULK1 dysregulation has recently been found in several human cancers.

Methods: mRNA expression levels of ULK1 and clinical information were analysed from The Cancer Genome Atlas data. ULK1 expression levels were verified in 36 paired fresh ccRCC tissue specimens by western blot analysis. Expression of ULK1 was knocked down by shRNA lentivirus. ULK1 activity was inhibited by SBI-0206965. The effect of inhibition of ULK1 was measured by detecting the apoptotic rate, autophagy, and the ratio of ROS and NADPH. The efficacy of SBI-0206965 *in vivo* was assessed by the murine xenograft model.

Findings: *ULK1* mRNA expression was significantly upregulated in clear cell renal cell carcinoma (ccRCC) and overexpression of *ULK1* correlated with poor outcomes. We found that ULK1 was highly expressed in 66.7% of ccRCC tumours ($p < 0.05$). Knockdown of ULK1 and selective inhibition of ULK1 by SBI-0206965 induced cell apoptosis in ccRCC cells. We demonstrated that SBI-0206965 triggered apoptosis by preventing autophagy and pentose phosphate pathway (PPP) flux. Furthermore, blocking the kinase activity of ULK1 with SBI-0206965 resulted in a level of anticancer effect *in vivo*.

Interpretation: Taken together, our results suggested that ULK1 was upregulated in ccRCC tumours and may be a potential therapeutic target. Therefore, SBI-0206965 should be further considered as an anti-ccRCC agent.

Fund: This work was supported in part by The National Natural Science Foundation of China (No. 81570748) and Natural Science Foundation of Fujian Province (No. 2018J01345, 2017XQ1194).

© 2018 The Authors. Published by Elsevier B.V. This is an open access article under the CC BY-NC-ND license (<http://creativecommons.org/licenses/by-nc-nd/4.0/>).

* Corresponding authors at: Fuzhou General Hospital or Dongfang Hospital, Xiamen University, Fuzhou, China.

E-mail addresses: junlu.heather@xmu.edu.cn (J. Lu), 13905915547@163.com (W. Wu), tanjm156@xmu.edu.cn (J. Tan).

¹ These authors have contributed equally to this work.

Research in context

Evidence Before This Study

Elevated ULK1 expression has been observed in human cancers, including nasopharyngeal carcinoma, oesophageal squamous cell carcinoma, colorectal cancer, and hepatocellular carcinoma. Egan et al. developed SBI-0206965, a selective small molecule inhibitor of ULK1 kinase in 2015. They found that SBI-0206965 inhibits autophagy and enhances apoptosis in human glioblastoma and lung cancer cells. Recent studies showed that SBI-0206965 could suppress phosphorylation of the β 1-Ser108 of AMP-activated protein kinase (AMPK), and induce cell apoptosis and enhance the sensitivity of cisplatin against non-small cell lung cancer cells. However, to date, the exact expression profile of ULK1 and the biological mechanism of SBI-0206965 in human ccRCC have not been determined. Added Value of This Study

In TCGA KIRC cohorts, ULK1 is highly expressed in renal clear cell carcinoma tissues, and its expression is positively correlated with the patient's survival time. We observed that ULK1 expression was upregulated in 66.7% of our fresh ccRCC tissues ($p < 0.05$). Knockdown of ULK1 and selective inhibition of ULK1 by SBI-0206965 under starvation conditions induced cell apoptosis in ccRCC cells. Then, we demonstrated that SBI-0206965 triggered apoptosis by preventing autophagy and pentose phosphate pathway (PPP) flux. Furthermore, SBI-0206965 resulted in a level of anticancer effect *in vivo* in a murine xenograft model. Implications of All the Available Evidence

Our results suggested that ULK1 may be a potential therapeutic target, and SBI-0206965 should be further considered as an anti-ccRCC agent.

1. Introduction

Clear cell renal cell carcinoma (ccRCC) is the most common type of renal malignancy, being responsible for approximately 75% of all cases of renal cell carcinoma (RCC) [1]. Compared with that of other subtypes of RCC, ccRCC is characterized by high metastasis and rates of relapse. Almost 30% of new ccRCC cases have metastasised by the time of diagnosis and will suffer from recurrence after resection [2]. The 5-year overall survival rate of metastatic RCC is only 10%, which is in contrast to that of non-metastatic RCC with an estimated rate of over 55% [3]. Therapeutic agents such as sorafenib [4], sunitinib [5], everolimus [6], bevacizumab [7], and pazopanib [8] produce partial improvement for ccRCC patients, but the efficacy of these drugs for metastatic RCC remains limited [9, 10]. Therefore, there is a need to identify novel biomarkers for predicting the progression and prognosis of ccRCC and to develop novel treatment strategies.

Previous studies of budding yeast demonstrated that autophagy related 1 (ATG1) is one of the upstream components of the autophagy pathway [11, 12]. In mammals, ATG1 has two homologous [13], uncoordinated 51-like kinase 1 (ULK1) and ULK2, which initiate autophagy in response to starvation [14]. ULK1 and ULK2 also phosphorylate key glycolytic enzymes to promote additional carbon flux into PPP during times of nutritional stress in order to maintain redox homeostasis. Knockdown of ULK1 and ULK2 leads to decreased NADPH/NADP⁺ ratios and lower percentages of cell death [15].

Elevated ULK1 expression has been observed in human cancers, including nasopharyngeal carcinoma [16], oesophageal squamous cell carcinoma [17], colorectal cancer [18], and hepatocellular carcinoma

[19] and is an independent predictor of poor survival for patients with these cancers. A recent study analysed the prognostic significance of five autophagy-related proteins in specimens from patients with metastatic RCC receiving mammalian target of rapamycin (mTOR) inhibitors as treatment and found that ULK1 expression correlates with the response to everolimus or temsirolimus [20]. Egan et al. developed SBI-0206965, a selective small molecule inhibitor of ULK1 kinase. SBI-0206965 inhibits autophagy and enhances apoptosis in human glioblastoma and lung cancer cells, suggesting it has therapeutic potential [21]. SBI-0206965 also suppresses phosphorylation of the β 1-Ser108 of AMP-activated protein kinase (AMPK), which has been demonstrated to upregulate pro-survival pathways [22]. Recently, Tang et al. showed that SBI-0206965 induces cell apoptosis and enhances the sensitivity of cisplatin against non-small cell lung cancer cells [23]. However, to date, the exact expression profile of ULK1 and the biological mechanism of SBI-0206965 in human ccRCC have not been determined.

In this study, we investigated the expression pattern of ULK1 and the antitumor effects of SBI-0206965 on ccRCC. Upregulation of ULK1 at the protein level was confirmed in 36 freshly collected ccRCC samples. SBI-0206965 appeared to increase apoptosis by inhibiting cell autophagy and by increasing the levels of reactive oxygen species (ROS) in ccRCC cells. In a xenograft mouse model, SBI-0206965 inhibited tumour growth without producing any symptoms of toxicity. Results from this work revealed that ULK1 may be a novel prognostic marker and suggests that SBI-0206965 may be a potential therapeutic agent for ccRCC.

2. Materials and Methods

2.1. Analysis of the Cancer Genome Atlas (TCGA) Data of ccRCC

Published mRNA expression data for 72 normal kidney tissues and 524 ccRCC specimens were downloaded from TCGA (<http://cancergenome.nih.gov>) on July 2016. Differential gene expression was analysed using R and Bioconductor software. Kaplan–Meier survival curves were generated for ccRCC patients entered in the TCGA database (<http://www.oncolnc.org/>).

2.2. Clinical Specimens

Thirty-six ccRCC tissue specimens and their matched normal adjacent tissues located >2 cm from the edge of the cancer tissue were obtained from patients at Fuzhou General Hospital from November 2013 to November 2015. The collection and use of the tissue specimens were approved by the Human Research Ethics Review Committee of Fuzhou General Hospital (No. 2013–017). All patients provided written informed consent. Table 1 lists the demographic details of the patients.

2.3. Cell Culture

The ccRCC cell lines A498 and ACHN were obtained from GeneChem (Shanghai, China). Normal human lung cell line HKC and HEK293T were obtained from the Chinese Academy of Sciences Committee Typical Culture Collection Cell Bank (Shanghai, China). Cells were grown in RPMI-1640 medium, supplemented with 10% (v/v) fetal bovine serum (FBS) and 1 × penicillin/streptomycin (Thermo Fisher Scientific, USA). All the cells were cultured at 37 °C in a humidified incubator with 5% CO₂.

2.4. Plasmids and Transfection

Plasmid pEGFP-LC3 was derived from the Addgene plasmid 22,564. Lentiviral vectors pLKO.1-shRNA-ULK1 (clone ID TRCN0000000835) and SHC002 (pLKO.1-puro Non-Mammalian shRNA Control Plasmid) were obtained from Sigma-Aldrich (St. Louis, MO, USA). For virus packaging, the non-targeting sequence control or shRNA constructs were co-transfected with pMD2.G and psPax2 into HEK293T cells using FuGENE HD (Promega, Madison, USA). A498 and ACHN cells were

Table 1
List of 36 clear cell renal cell carcinoma tissues.

Characteristics	N(%)
Gender	
Male	26 (72.2%)
Female	10 (27.8%)
Age at surgery	
<60	23 (63.9%)
≥60	13 (36.1%)
Tumour extent	
T1	23 (63.9%)
T2	11 (30.6%)
T3	1 (2.8%)
T4	1 (2.8%)
Lymph node metastasis	
N0	31 (86.1%)
≥N1	5 (13.9%)
Distant metastasis	
M0	32 (88.9%)
M1	4 (11.1%)
Tumour max diameter (cm)	
<7	29 (80.6%)
≥7	7 (19.4%)
Fuhrman grade b	
G1	11 (30.6%)
G2	23 (63.9%)
G3	2 (5.6%)
G4	0

infected with virus-containing media. The sequence with higher knock-down efficiencies was selected based on the five shRNA sequences of ULK1. Inhibition efficiency of gene expression detected by quantitative PCR (data not shown) and verified by western blot assay.

2.5. Western Blotting

Cell extracts were prepared by lysing cells with lysis buffer (Beyotime, Shanghai, China). Total protein concentrations were determined using a Pierce BCA Protein Assay Kit (Thermo Fisher Scientific). The protein samples (50 µg) were separated using 10% sodium dodecyl sulphate-polyacrylamide gel electrophoresis (SDS-PAGE) and then transferred to polyvinylidene fluoride membranes (Immobilon-P PVDF Membrane; EMD Millipore). After blocking, the membranes were probed with primary antibodies overnight at 4 °C. The following day, the membranes were incubated at room temperature for 1 h with horseradish peroxidase (HRP)-conjugated secondary IgG antibodies. The protein bands were visualized using SuperSignal West Pico Chemiluminescent Substrate (Pierce; Thermo Fisher Scientific, Inc., Waltham, MA, USA) and exposure to X-ray film. ACTIN was used as an internal loading control. The intensities of the bands were quantified using ImageJ software. The antibodies used are listed in Table S1.

2.6. Cell Death Detection by ELISA

A498 and ACHN cells (1×10^5 /well) were evenly distributed and grown in 100-mm culture dishes overnight and then treated with Earle's Balanced Salt Solution (EBSS) and SBI-0206965 (Cat. No. HY-16966, MedChem Express, Shanghai, China) at various concentrations (0, 5, 10, and 20 µg/mL) or chloroquine (CQ; Cat. No. C6628; Sigma-Aldrich) for 24 h. Cells were harvested and assayed using a Cell Death Detection ELISA Kit (Cat. No. 11544675001, Roche, Switzerland) following the manufacturer's instructions.

2.7. Measurement of ROS Levels

A498 and ACHN cells (1×10^5 /well) were grown in 100-mm culture dishes overnight and then treated with EBSS containing 10 µM SBI-0206965. Thirty min prior to harvesting, 20 µM 2,7-dichloro-4,6-diamidino-2-phenylindole diacetate (DCFH-DA; Sigma-Aldrich) was

added to each culture. The fluorescence intensity was analysed using a flow cytometer (BD Biosciences).

2.8. Measurement of NADPH and NADP

Levels of NADPH and NADP⁺ were measured using a NADP/NADPH Quantitation Kit (Sigma-Aldrich, USA) following the manufacturer's instructions. In brief, the cells were treated with EBSS and 10 µM SBI-0206965. The cells were then treated with NADP/NADPH extraction buffer and the NADPH developer was added. The reaction mixture was incubated at room temperature for 1 h. The samples were analysed at an absorbance at 450 nm using a spectrophotometer.

2.9. Xenograft Model

Six-week-old male BALB/c nude mice were provided by the Shanghai Laboratory Animal Center (Shanghai, China). A498 cells (5×10^6) suspended in 100 µL PBS/Matrigel (1:1) were injected into the hind flank of the mice. The mice were randomly divided 14-d post implantation into two groups of six mice each. Mice were intraperitoneally injected with dimethyl sulfoxide (DMSO) used as the vehicle solution or SBI-0206965 in DMSO (50 mg/kg/d) every 3 d for a total of nine times over a 30-d period. Tumour growth was evaluated every 3 d. Tumour volume was calculated using the formula $\text{volume} = 1/2 (\text{length} \times \text{width}^2)$. At the end of the experiment, the mice were sacrificed by cervical dislocation and tumours were harvested. The tumour specimens were fixed in 4% paraformaldehyde, paraffin embedded, and sectioned. The tissue sections were analysed by terminal deoxynucleotidyl transferase dUTP nick end labelling (TUNEL) assays. Mice were maintained in the specific-pathogen-free (SPF) Animal Research Centre of Fuzhou General Hospital. All animal studies were approved by the Ethics Committee for Animal Experimentation and Animal Welfare at the Fuzhou General Hospital (Fuzhou, China).

2.10. TUNEL Assay

TUNEL assays (Roche Diagnostics Corporation, USA) were performed according to the manufacturer's recommended protocol to detect DNA fragmentation during apoptosis induced by the SBI-0206965 treatment. In brief, the tissue sections were rehydrated in xylenes followed by isopropyl alcohol. The sections were then treated with 30 µg/mL proteinase K followed by incubation with 0.3% hydrogen peroxide for 30 min. The cells were then rinsed and incubated with TUNEL reaction mixture at room temperature for 30 min in the dark. The nuclei were counterstained with 4,6-diamidino-2-phenylindole (DAPI). TUNEL-positive cells were examined using an Olympus fluorescence microscope.

2.11. Statistical Analysis

SPSS 17.0 and GraphPad Prism 6.0 software was used for statistical analysis of the data. The results of the quantitative data are presented as the mean ± standard deviation (SD). Statistical differences between the groups were analysed with the Student's *t*-test. For multiple comparisons, one-way ANOVA, followed by *t*-test with the Bonferroni correction was performed. Differences were considered statistically significant at $p < 0.05$.

3. Results

3.1. Analysis of ULK1 Expression in ccRCC Patients

To analyse the role of ULK1 in ccRCC, ULK1 mRNA expression and clinical information were extracted from the publicly available TCGA dataset [24]. ULK1 gene expression was significantly elevated in the

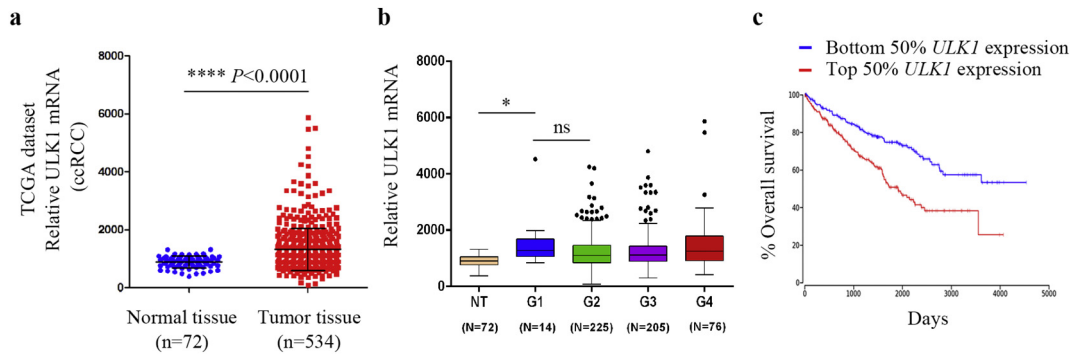


Fig. 1. Expression of *ULK1* mRNA and its association with overall survival in ccRCC based on analysis of The Cancer Genome Atlas (TCGA) data. (a) The relative mRNA expression of *ULK1* in ccRCC tissues was upregulated when compared with that in normal matched kidney tissues. The p value was measured with Student's *t*-tests. **** $p < 0.0001$. (b) Box plot of *ULK1* mRNA levels in non-tumorigenic tissues. Fuhrman tumour grade 1 (G1), 2 (G2), 3 (G3), and 4 (G4) of ccRCC patients. (c) Kaplan–Meier analysis of overall survival for ccRCC patients relative to expression levels of *ULK1*. Patients were stratified as low and high expression of *ULK1* mRNA (www.oncolnc.org). p-value = 3.04×10^{-6} vs. the *ULK1* low group.

ccRCC tumours compared to that in normal renal tissues (Fig. 1a). Significant differences in *ULK1* expression were observed between normal kidney tissue and ccRCC grade (G) 1, 2, 3, and 4 specimens. In contrast, expression of *ULK2*, another *ATG1* homologous gene, did not differ significantly compared to that of normal kidney tissue (Fig. S1a). However, *ULK1* expression did not show a stepwise increment from G1 to G4 (Fig. 1b). The ccRCC cases were assigned to a *ULK1*-low group (n =

261) or *ULK1*-high group (n = 261) based on their level of expression. Analysis of the results showed that high *ULK1* expression was related to shorter overall survival in ccRCC patients, indicating that overexpression of *ULK1* mRNA was correlated with poor outcome (Fig. 1c). High expression of *ULK2* did not appear to correlate with the overall survival rate in ccRCC patients (Fig. S1b). These data are consistent with overexpression of *ULK1* being important for the development of ccRCC.

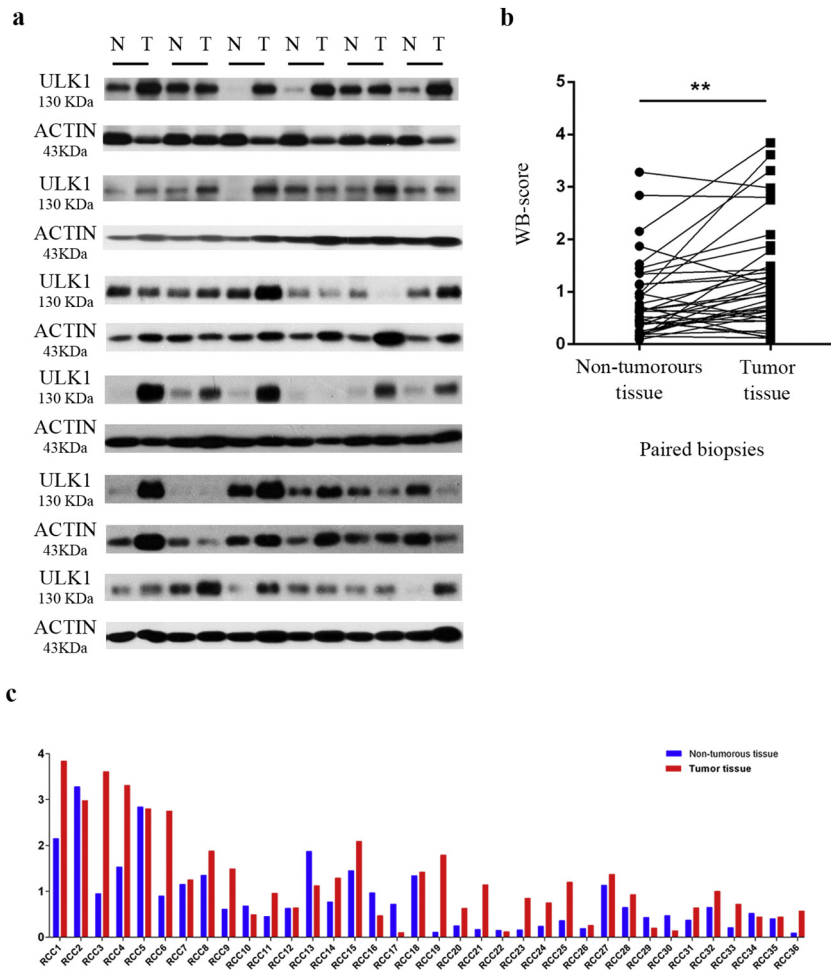


Fig. 2. *ULK1* was aberrantly upregulated in human ccRCC samples. (a) *ULK1* protein expression was detected by western blotting in 36 paired clinical ccRCC specimens and their matched adjacent non-tumorous tissues. (b) The paired sample *t*-test method was used to compare the differences in *ULK1* protein expression between the ccRCC specimens and matched adjacent non-tumorous tissues. The p value was measured with paired Student's *t*-tests. ** $p < 0.01$. Western blotting (WB) score: quantitative analysis of *ULK1*/ACTIN density ratios detected by western blotting. (c) The relative levels of *ULK1* expression in clinical ccRCC specimens and matched adjacent non-tumorous tissues were calculated. ACTIN was used as an internal control.

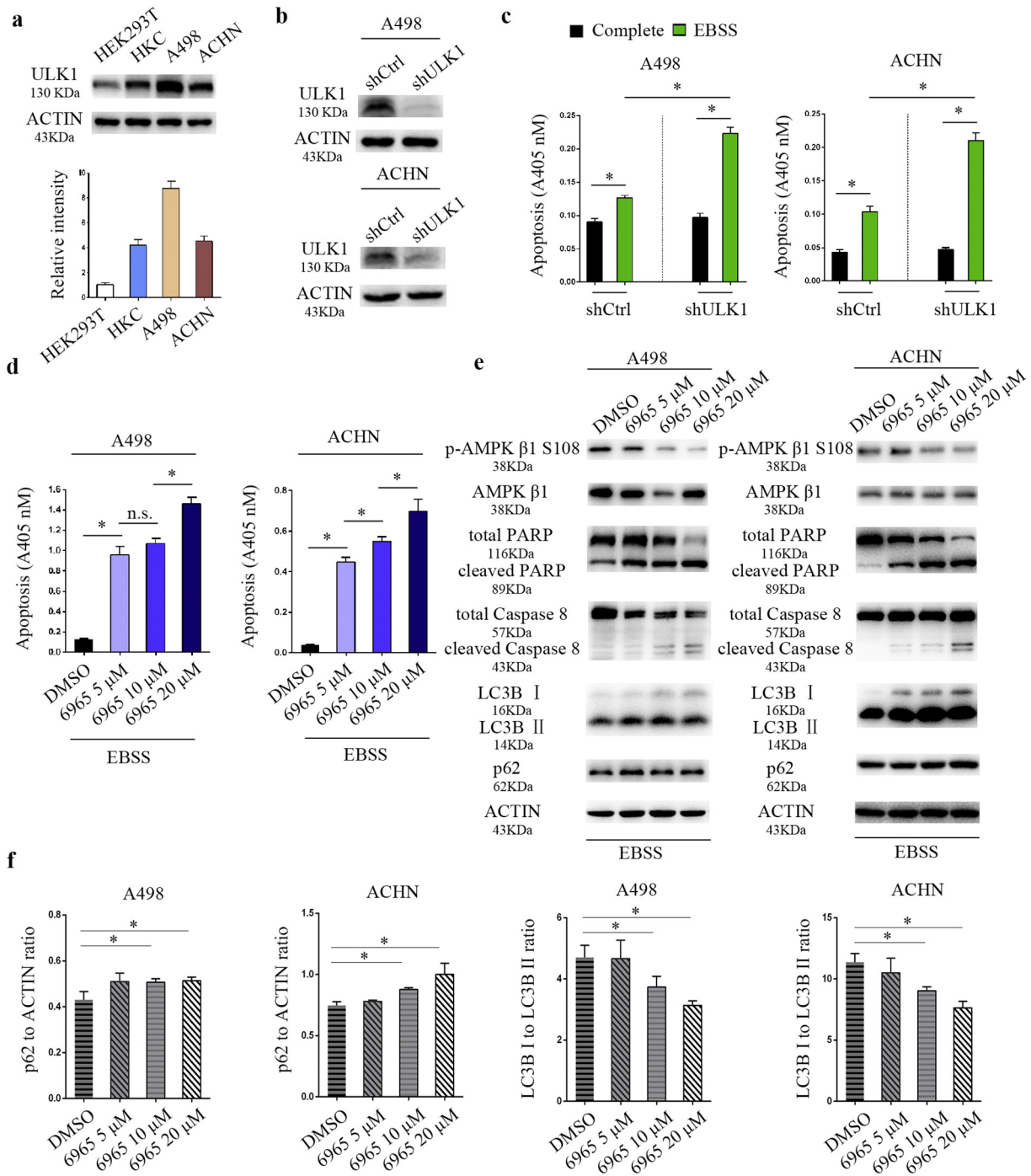


Fig. 3. Knockdown of ULK1 or its selective inhibition by treatment with SBI-0206965 induced cell apoptosis in ccRCC cells under conditions of starvation. (a) The expression of ULK1 was examined by western blot analysis in human ccRCC cell lines A498 and ACHN. The results shown are representative data from three independent experiments. (b) The expression of ULK1 in A498 and ACHN cells, as detected by western blotting, was efficiently downregulated following transfection with specific shRNA sequences. The results shown are representative of three independent experiments. (c) Transfected cells were cultured in regular medium or starvation medium (EBSS) for 24 h. Cell apoptosis was detected in three independent experiments using an ELISA-based cell apoptosis detection kit. The p-values were calculated for differences between the ccRCC cells transfected with the ULK1-specific shRNA sequences and the control shRNA sequences (shCtrl). The p value was measured with Student's *t*-tests. **p* < 0.05. (d) A498 and ACHN cells were cultured in starvation medium (EBSS) with various concentrations of SBI-0206965 (0 μM, 5 μM, 10 μM, and 20 μM) for 24 h. Cell apoptosis was evaluated using an ELISA-based cell apoptosis detection kit. The p value was measured with Student's *t*-tests. **p* < 0.05, compared with that of DMSO-treated vehicle control group (0 μM SBI-0206965). (e) A498 and ACHN cells were cultured in starvation medium (EBSS) with SBI-0206965 (0 μM, 5 μM, 10 μM, and 20 μM) for 24 h. Phosphorylation of Ser108 of the AMPK β1 subunit, cleavage of PARP and Caspase 8, and levels of LC3B and p62 were measured by western blot analysis. The results are representative of three independent experiments. (f) Western blot analysis of p62 and LC3B. The band intensities were quantified using ImageJ software. The amount of p62 was normalized to ACTIN. The relative amount of LC3B was determined as the LC3II/LC3I (II/I) ratio.

3.2. ULK1 Was Upregulated in ccRCC Tissues

To confirm the expression of ULK1, we performed western blotting analyses on 36 pairs of human ccRCC specimens and their matched adjacent normal renal tissues. Increased protein levels of ULK1 were

detected in 24 of the 36 (66.7%) tumour samples (Fig. 2a). Statistical analysis revealed that the expression of ULK1 was significantly upregulated in the ccRCC specimens compared to that of the adjacent normal tissues (Fig. 2b and c). These results suggested that ULK1 expression was aberrantly increased in a subset of ccRCC tumours.

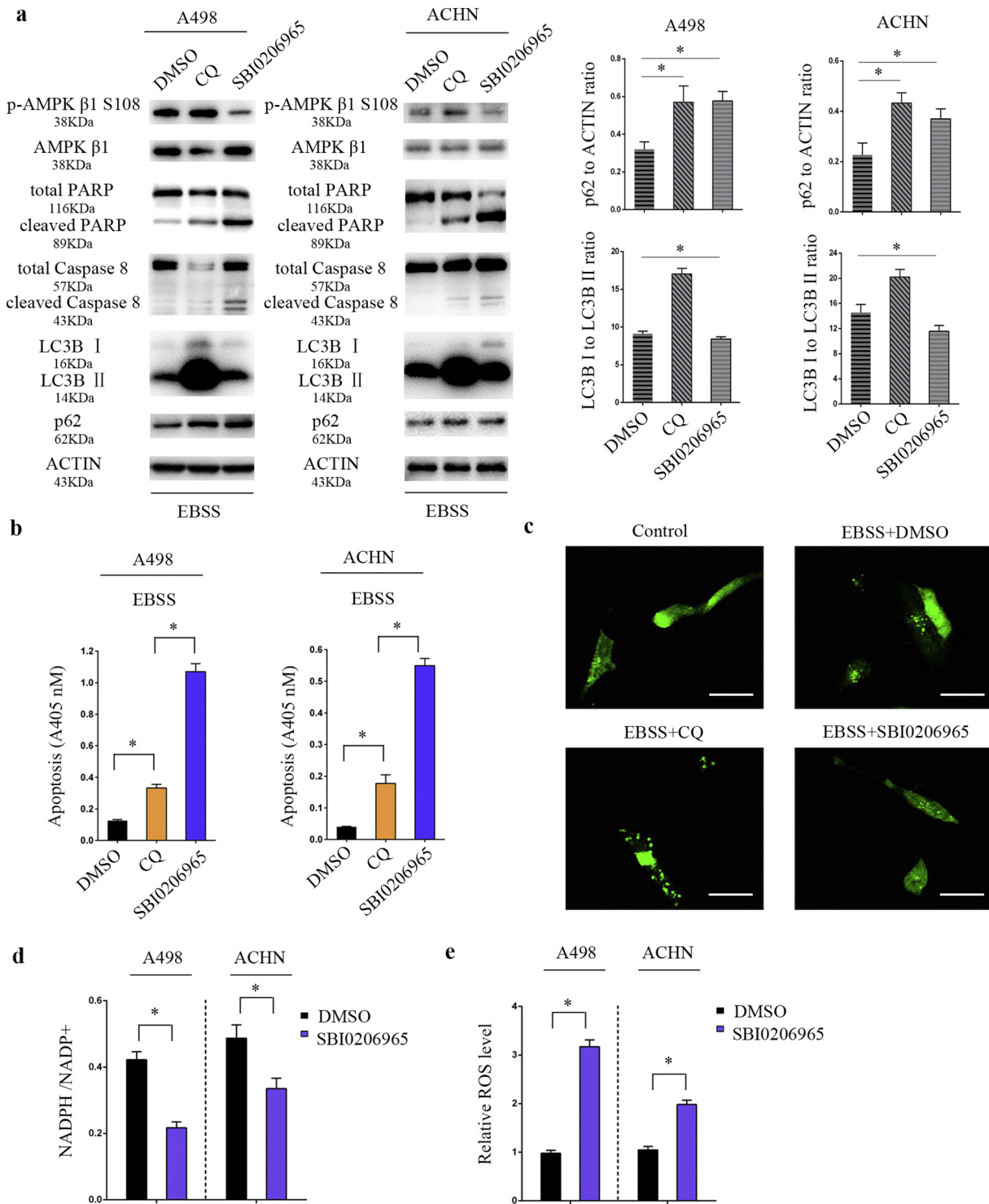


Fig. 4. SBI-0206965 promoted apoptosis in ccRCC cells through inhibition of PPP and autophagy. (a) A498 and ACHN cells were cultured in starvation medium (EBSS) with 10 μ M chloroquine (CQ) or 10 μ M SBI-0206965 for 24 h. Western blot analysis of AMPK β 1, PARP, Caspase 8, LC3B, and p62 was performed. The amount of p62 was normalized to ACTIN. The relative amount of LC3B was determined as the LC3II/LC3I (II/I) ratio. The results shown are representative of three independent experiments. (b) A498 and ACHN cells were cultured in starvation medium (EBSS) with 10 μ M CQ or 10 μ M SBI-0206965 for 24 h. Cell apoptosis was detected using an ELISA-based cell apoptosis detection kit. The p value was measured with Student's *t*-tests. **p* < 0.05, compared with that of the DMSO-treated control group. (c) SBI-0206965 prevented the translocation of EGFP-LC3. ACHN cells were transduced with a plasmid expressing EGFP-LC3. Transduced cells were either left in growth medium, or nutritionally stressed in EBSS in the presence or absence of chloroquine and SBI-0206965 for 12 h. Cells were visualized using an Olympus Fluoview FV1000 laser scanning confocal microscope. The results shown are representative of three independent experiments. Scale bars, 20 μ m. (d) A498 or ACHN cells incubated in EBSS with or without 10 μ M SBI-0206965 for 24 h. The NADPH/NADP⁺ ratios were measured in three independent experiments. p-values were calculated compared with that of the DMSO-treated controls, and measured with Student's *t*-tests. **p* < 0.05. (e) A498 or ACHN cells were incubated in EBSS with or without 10 μ M SBI-0206965 for 24 h. The levels of ROS were determined using flow cytometry and the results are shown in the histograms. p-values were calculated compared with that of the DMSO-treated controls, and measured with Student's *t*-tests. **p* < 0.05.

3.3. Inhibition of ULK1 Kinase Activity Induced Apoptosis of ccRCC Cells During Starvation

We evaluated ULK1 expression levels in immortalized human renal cell lines HEK293T and HKC and the two ccRCC cell lines A498 and ACHN (Fig. 3a). ULK1 activity plays a vital role in autophagy-mediated survival [25] and maintaining redox balance by allocating glucose flux to PPP during nutritional stress [15]. Therefore, ULK1 activity may contribute to the survival of ccRCC cells under amino acid and serum starvation conditions.

To assess the effects of ULK1 on cell survival during nutritional stress, A498 and ACHN cells were transfected with ULK1-specific shRNA plasmids or negative control shRNA plasmid (shCtrl) and then nutritionally stressed with EBSS (Fig. 3b). The rate of cell apoptosis was measured by ELISA. We detected a significant increase in the rate of cell death when

ULK1 was downregulated in both ccRCC cell lines under starvation conditions ($p < 0.01$) (Fig. 3c). The effects of the selective ULK1 inhibitor SBI-0206965 on cell apoptosis and autophagy were also evaluated under EBSS treatment in human ccRCC cell lines A498 and ACHN. Cell apoptosis was measured by ELISA and Annexin V-FITC/PI assay. Findings from ELISA showed that SBI-0206965 treatment induced significant levels of apoptosis in both ccRCC cell lines (Fig. 3d). All three doses of SBI-0206965 dramatically increased the rate of cell death. Flow cytometry analysis also demonstrated enhanced levels of cell death with increasing concentrations of SBI0206965 in ACHN and A498 cells (Fig. S2a). Treatment with SBI0206965 attenuated the phosphorylation of Ser108 of the AMPK β 1 subunit, suggesting that ULK1 kinase activity was inhibited by SBI0206965 (Fig. 3e). Autophagy was evaluated by analysis of LC3B and p62 using western blotting. A concentration-dependent decrease in the conversion of LC3B I to LC3B II was observed

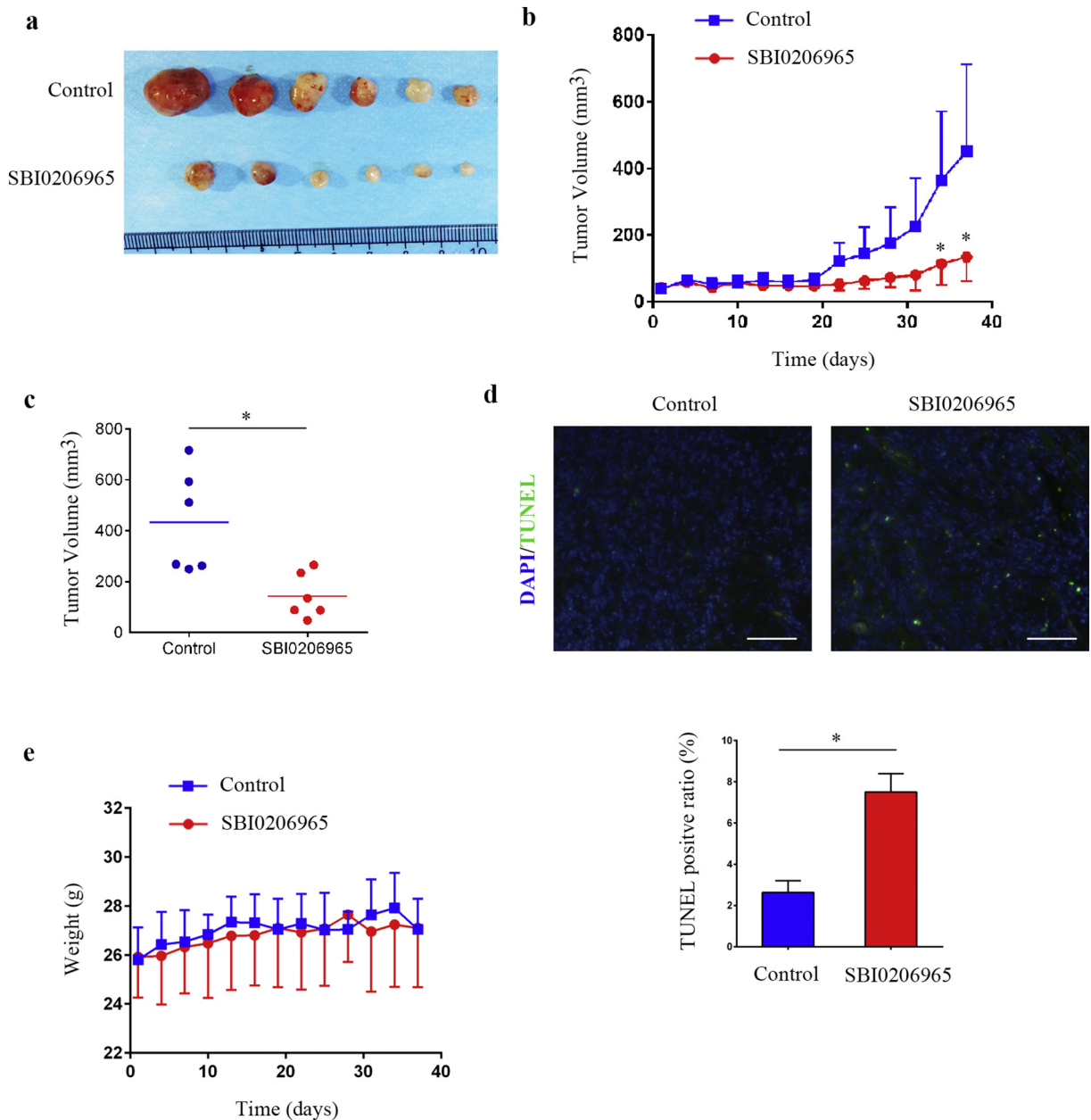


Fig. 5. SBI-0206965 inhibited the growth of A498-derived xenograft tumours. (a) Representative images of A498 xenograft tumours in BALB/c nude mice intraperitoneally injected with vehicle (DMSO) or SBI-0206965. (b) Growth curves of the xenograft tumours in BALB/c nude mice (n = 6 per group). (c) Tumour volume of xenografts derived from A498 cells. The p value was measured with Student's *t*-tests. * $p < 0.01$. (d) Representative staining by TUNEL assays in each group. All green-fluorescent bodies in the tumour samples were TUNEL-positive cells. Figures were photographed using an Olympus X81 microscope. Scale bars, 50 μ m. (e) BALB/c nude mice body weight during treatment with SBI-0206965 or DMSO vehicle (n = 6 per group).

in both A498 and ACHN cells (Fig. 3e). The quantitative data are shown in Fig. 3F. SBI0206965 increased the levels of cleaved Caspase 8 and PARP, markers of apoptosis (Fig. 3e). Under normal conditions, SBI0206965 was able to induce apoptosis (Fig. S2b) but the activity of SBI0206965 was more pronounced under conditions of starvation.

3.4. SBI-0206965 Induced ccRCC Cells Apoptosis Through Autophagy and PPP Inhibition

Our experimental findings demonstrated that SBI-0206965 inhibited autophagy, as evidenced by increased levels of LC3B I and the autophagy substrate p62 (Fig. 4a). Chloroquine inhibits autophagy by inhibiting autophagosome and lysosomal fusion (Maycotte et al., 2012), so its treatment significantly increased the abundance of green fluorescent protein (GFP) labelled-LC3B spots (Fig. 4c). The LC3B puncta represented the basal steady-state levels of autophagosomes. When ccRCC cells were treated with SBI-0206965 the autophagosomes were almost absent (Fig. 4c). However, chloroquine treatment resulted in less Caspase 8 and PARP cleavage and lower rates of cell death (Fig. 4a and b), suggesting that ULK1 exerts oncogenic activity, not only through autophagy, but also through other pathways. Li et al. discovered that the depletion of ULK kinase reduces PPP activity, as well as the level of ROS. Thus, we focused on intracellular NADPH/NADP⁺ and ROS levels. We found that SBI-0206965 treatment decreased the ratio of NADPH/NADP⁺ (Fig. 4d). Moreover, SBI-0206965 clearly influenced ROS levels compared with that of the DMSO-treated control group (Fig. 4e). Taken together, SBI-0206965 induced apoptosis of ccRCC cells through inhibiting autophagy and decreasing the rate of ROS clearance under conditions of starvation.

3.5. SBI-0206965 Inhibited Tumour Growth and Induced Apoptosis In Vivo

To evaluate the anti-tumour efficacy *in vivo*, nude mice inoculated subcutaneously with A498 cells were intraperitoneally injected with either vehicle (DMSO) or SBI-0206965 (50 mg/kg) once every three days for 37 d starting 14 d after injection of the ccRCC cells. The A498 xenograft tumour growth rate was significantly suppressed by SBI-0206965 compared with that of the vehicle (Fig. 5a, b, and c). In contrast, no significant differences in weight of the mice were observed comparing the vehicle control and SBI-0206965 groups (Fig. 5e). Mice in the SBI-0206965 group did not display signs of toxicity such as agitation, indigestion, or diarrhoea, impaired movement or posture, or areas of redness or swelling. Moreover, treatment with SBI-0206965 did not affect the renal structure in mice (Fig. S2).

To evaluate the effect of SBI-0206965 on induction of apoptosis in A498 xenograft tumours, TUNEL analyses were performed on tissue sections. Treatment of mice with SBI-0206965 resulted in increased cell apoptosis in the tumour samples, as demonstrated by more green-coloured apoptotic cells (Fig. 5d). Such findings suggest that SBI-0206965 mediated anti-tumour effects *in vivo*.

4. Discussion

ULK1 is essential to the initial stages of autophagy [25], but the role of ULK1 in cancer is not currently clear. It has been shown that ULK1 is induced by hypoxia and that ablation of ULK1 causes death of cancer cells under conditions of both normoxia and hypoxia [26]. High expression of ULK1 correlates to prognosis in certain malignant tumours. However, in other cancer cell types ULK1 promotes cell apoptosis [27–29]. In the current study, we determined that ULK1 expression was upregulated in ccRCC tissue and correlated with prognosis. Inhibition of ULK1 by knockdown or by treatment with SBI-0206965 promoted cell apoptosis in ccRCC cells. Therefore, ULK1 may contribute to tumorigenesis and the progression of ccRCC.

Another important phenomenon observed in the current study was that treatment with SBI-0206965 inhibited autophagy and induced

apoptosis in ccRCC cells, whereas chloroquine, a classic autophagy inhibitor [30, 31], caused less Caspase 8 and PARP cleavage and cell death during EBSS treatment. We detected a significant autophagy inhibition after chloroquine treatment, rather than after treatment with SBI-0206965, indicating that ULK1 exerts carcinogenic effects not only through autophagy but also through other means. The current results indicate that ULK1 and ULK2 directly phosphorylated key glycolytic enzymes leading to repartition and additional carbon flux to PPP [15], which branches from glycolysis at the first committed step of glucose metabolism. PPP is considered to be a major contributor of equivalents in the form of reduced NADPH for intracellular ROS homeostasis [32, 33]. It is becoming clearer that PPP plays an essential role in regulating cancer cell growth [34]. Dysregulation of PPP metabolic flux strikingly impacts cancer growth and cell survival. Our study showed that SBI-0206965 treatment elevated levels of ROS in starved ccRCC cells and increased the rate of cell death, providing evidence that SBI-0206965 may suppress PPP flux. However, due to the inability to obtain antibodies, our results lack evidence that SBI-0206965 affects the level of glycolytic enzyme phosphorylation, which requires further study. In addition, SBI-0206965 has also been shown to inhibit the phosphorylation of AMPK β 1 [22]. We cannot completely rule out the possibility that SBI-0206965 inhibits other kinases to promote apoptosis in this study.

Mammals have five ULK1 homologs: ULK1, ULK2, ULK3, ULK4, and serine/threonine kinase 36 (STK36) [12]. ULK1 and ULK2 appear to perform redundant roles in autophagy [13, 35]. However, ULK2 also has some functions different from ULK1. Ro et al. showed that *ULK1* knockdown reduces fatty acid oxidation and elevates fatty acid uptake in adipocytes, whereas *ULK2* knockdown has the opposite effects [36]. Our study showed that the expression of ULK2 was not enhanced in ccRCC; in fact, ULK2 expression was not even detectable in A498 cells (data not shown). Thus, the current study examined only the function of ULK1.

Supplementary data to this article can be found online at <https://doi.org/10.1016/j.ebiom.2018.07.034>.

Declaration of Interests

There are no conflicts of interest among the authors.

Author Contributions

Jun Lu designed the study, analysed the data, and wrote the paper. Ling Zhu, Luoping Zheng, and Qiang Cui performed the experiments and collected and analysed the data. Hu Zhao, Huiyue Dong, and Zhouji Shen performed the statistical analysis. Hehuan Zhu and Zhan Chen performed the animal studies. Shushang Chen and Weizhen Wu provided the ccRCC patient samples. Jianming Tan supervised the study, analysed the data, and edited the manuscript.

Acknowledgement

We thank all the study participants. This work was supported in part by The National Natural Science Foundation of China (No. 81570748) and Natural Science Foundation of Fujian Province (No. 2018J01345, 2017XQ1194).

References

- [1] Shuch, B., Amin, A., Armstrong, A.J., Eble, J.N., Ficarra, V., Lopez-Beltran, A., et al., 2015]. Understanding pathologic variants of renal cell carcinoma: distilling therapeutic opportunities from biologic complexity. *Eur Urol* 67, 85–97.
- [2] Ljungberg, B., Bensalah, K., Canfield, S., Dabestani, S., Hofmann, F., Hora, M., et al., 2015]. EAU guidelines on renal cell carcinoma: 2014 update. *Eur Urol* 67, 913–924.
- [3] Leibovich, B.C., Lohse, C.M., Crispen, P.L., Boorjian, S.A., Thompson, R.H., Blute, M.L., et al., 2010]. Histological subtype is an independent predictor of outcome for patients with renal cell carcinoma. *J Urol* 183, 1309–1315.
- [4] Escudier, B., Eisen, T., Stadler, W.M., Szczylik, C., Oudard, S., Siebels, M., et al., 2007]. Sorafenib in advanced clear-cell renal-cell carcinoma. *N Engl J Med* 356, 125–134.

- [5] Motzer, R.J., Hutson, T.E., Tomczak, P., Michaelson, M.D., Bukowski, R.M., Rixe, O., et al., 2007]. Sunitinib versus interferon alfa in metastatic renal-cell carcinoma. *N Engl J Med* 356, 115–124.
- [6] Motzer, R.J., Escudier, B., Oudard, S., Hutson, T.E., Porta, C., Bracarda, S., et al., 2008]. Efficacy of everolimus in advanced renal cell carcinoma: a double-blind, randomised, placebo-controlled phase III trial. *Lancet* 372, 449–456.
- [7] Escudier, B., Pluzanska, A., Koralewski, P., Ravaud, A., Bracarda, S., Szczylik, C., et al., 2007]. Bevacizumab plus interferon alfa-2a for treatment of metastatic renal cell carcinoma: a randomised, double-blind phase III trial. *Lancet* 370, 2103–2111.
- [8] Sternberg, C.N., Davis, I.D., Mardiak, J., Szczylik, C., Lee, E., Wagstaff, J., et al., 2010]. Pazopanib in locally advanced or metastatic renal cell carcinoma: results of a randomised phase III trial. *J Clin Oncol* 28, 1061–1068.
- [9] Jonasch, E., Gao, J., Rathmell, W.K., 2014]. Renal cell carcinoma. *BMJ* 349, g4797.
- [10] Buchler, T., Bortlicek, Z., Poprach, A., Pavlik, T., Veskrnova, V., Honzirkova, M., et al., 2016]. Outcomes for patients with metastatic renal cell carcinoma achieving a complete response on targeted therapy: a registry-based analysis. *Eur Urol* 70, 469–475.
- [11] Egan, D., Kim, J., Shaw, R.J., Guan, K.L., 2011]. The autophagy initiating kinase ULK1 is regulated via opposing phosphorylation by AMPK and mTOR. *Autophagy* 7, 643–644.
- [12] Mizushima, N., 2010]. The role of the Atg1/ULK1 complex in autophagy regulation. *Curr Opin Cell Biol* 22, 132–139.
- [13] Alers, S., Löffler, A.S., Paasch, F., Dieterle, A.M., Keppeler, H., Lauber, K., et al., 2011]. Atg13 and FIP200 act independently of Ulk1 and Ulk2 in autophagy induction. *Autophagy* 7, 1423–1433.
- [14] Hosokawa, N., Hara, T., Kaizuka, T., Kishi, C., Takamura, A., Miura, Y., et al., 2009]. Nutrient-dependent mTORC1 association with the ULK1-Atg13-FIP200 complex required for autophagy. *Mol Biol Cell* 20, 1981–1991.
- [15] Li, T.Y., Sun, Y., Liang, Y., Liu, Q., Shi, Y., Zhang, C.S., et al., 2016]. ULK1/2 constitute a bifurcate node controlling glucose metabolic fluxes in addition to autophagy. *Mol Cell* 62, 359–370.
- [16] Yun, M., Bai, H.Y., Zhang, J.X., Rong, J., Weng, H.W., Zheng, Z.S., et al., 2015]. ULK1: a promising biomarker in predicting poor prognosis and therapeutic response in human nasopharyngeal carcinoma. *PLoS One* 10, e0117375.
- [17] Jiang, S., Li, Y., Zhu, Y.H., Wu, X.Q., Tang, J., Li, Z., et al., 2011]. Intensive expression of UNC-51-like kinase 1 is a novel biomarker of poor prognosis in patients with esophageal squamous cell carcinoma. *Cancer Sci* 102, 1568–1575.
- [18] Zou, Y., Chen, Z., He, X., He, X., Wu, X., Chen, Y., et al., 2015]. High expression levels of unc-51-like kinase 1 as a predictor of poor prognosis in colorectal cancer. *Oncol Lett* 10, 1583–1588.
- [19] Xu, H., Yu, H., Zhang, X., Shen, X., Zhang, K., Sheng, H., et al., 2013]. UNC51-like kinase 1 as a potential prognostic biomarker for hepatocellular carcinoma. *Int J Clin Exp Pathol* 6, 711–717.
- [20] Nishikawa, M., Miyake, H., Bing, L., Fujisawa, M., 2015]. UNC-51-like kinase 1 expression in radical nephrectomy specimens as a predicting factor of progression-free survival in patients with metastatic renal cell carcinoma treated with mammalian target of rapamycin inhibitors. *Urol Oncol* 33, 506 (e501–507).
- [21] Egan, D.F., Chun, M.G., Vamos, M., Zou, H., Rong, J., Miller, C.J., et al., 2015]. Small molecule inhibition of the autophagy kinase ULK1 and identification of ULK1 substrates. *Mol Cell* 59, 285–297.
- [22] Dite, T.A., Ling, N.X.Y., Scott, J.W., Hoque, A., Galic, S., Parker, B.L., et al., 2017]. The autophagy initiator ULK1 sensitizes AMPK to allosteric drugs. *Nat Commun* 8, 571.
- [23] Tang, F., Hu, P., Yang, Z., Xue, C., Gong, J., Sun, S., et al., 2017]. SBI0206965, a novel inhibitor of Ulk1, suppresses non-small cell lung cancer cell growth by modulating both autophagy and apoptosis pathways. *Oncol Rep* 37, 3449–3458.
- [24] Cancer Genome Atlas Research N., 2013]. Comprehensive molecular characterization of clear cell renal cell carcinoma. *Nature* 499, 43–49.
- [25] Wong, P.M., Puente, C., Ganley, I.G., Jiang, X., 2013]. The ULK1 complex: sensing nutrient signals for autophagy activation. *Autophagy* 9, 124–137.
- [26] Pike, L.R., Singleton, D.C., Buffa, F., Abramczyk, O., Phadwal, K., Li, J.L., et al., 2013]. Transcriptional up-regulation of ULK1 by ATF4 contributes to cancer cell survival. *Biochem J* 449, 389–400.
- [27] Gao, W., Shen, Z., Shang, L., Wang, X., 2011]. Upregulation of human autophagy-initiation kinase ULK1 by tumor suppressor p53 contributes to DNA-damage-induced cell death. *Cell Death Differ* 18, 1598–1607.
- [28] Joshi, A., Iyengar, R., Joo, J.H., Li-Harms, X.J., Wright, C., Marino, R., et al., 2016]. Nuclear ULK1 promotes cell death in response to oxidative stress through PARP1. *Cell Death Differ* 23, 216–230.
- [29] Jung, C.H., Seo, M., Otto, N.M., Kim, D.H., 2011]. ULK1 inhibits the kinase activity of mTORC1 and cell proliferation. *Autophagy* 7, 1212–1221.
- [30] Maycotte, P., Aryal, S., Cummings, C.T., Thorburn, J., Morgan, M.J., Thorburn, A., 2012]. Chloroquine sensitizes breast cancer cells to chemotherapy independent of autophagy. *Autophagy* 8, 200–212.
- [31] Rubinsztein, D.C., Gestwicki, J.E., Murphy, L.O., Klionsky, D.J., 2007]. Potential therapeutic applications of autophagy. *Nat Rev Drug Discov* 6, 304–312.
- [32] Kruger, N.J., von Schaeuwen, A., 2003]. The oxidative pentose phosphate pathway: structure and organisation. *Curr Opin Plant Biol* 6, 236–246.
- [33] Wamelink, M.M., Struys, E.A., Jakobs, C., 2008]. The biochemistry, metabolism and inherited defects of the pentose phosphate pathway: a review. *J Inherit Metab Dis* 31, 703–717.
- [34] Patra, K.C., Hay, N., 2014]. The pentose phosphate pathway and cancer. *Trends Biochem Sci* 39, 347–354.
- [35] Chan, E.Y., Tooze, S.A., 2009]. Evolution of Atg1 function and regulation. *Autophagy* 5, 758–765.
- [36] Ro, S.H., Jung, C.H., Hahn, W.S., Xu, X., Kim, Y.M., Yun, Y.S., et al., 2013]. Distinct functions of Ulk1 and Ulk2 in the regulation of lipid metabolism in adipocytes. *Autophagy* 9, 2103–2114.